National Conference with International Participation

ENGINEERING MECHANICS 2008

Svratka, Czech Republic, May 12 – 15, 2008

THE MOTION SIMULATION OF THE RAILWAY VEHICLE BOGIE EMPHATICALLY OF CREEP FORCE EFFECTS

J. Siegl[*], J. Švígler [**]

Summary: *The paper deals with the motion modelling of a material bogie of a railway vehicle. The aim of this contribution is the bogie motion analysis with consideration of creep force effects. The contact between the wheel sets and the railway is solved as a contact of two conical surfaces with two lines. The bogie suspension system is modeled by nonlinear suspension elements which are connected to the railway and the vehicle case. The railway and vehicle case is considered with no degrees of freedom. The comparison of the bogie motion without and with secondary suspension in the vehicle case is made. The solution is made for motion on the straight railway and constant forward velocity. The mathematical model of the railway vehicle bogie is created and the numerical solution of this mathematical model is made by own developed software which allows to simulate a bogie motion in dependence on initial values.*

1. Introduction

The paper deals with the motion modelling of a material bogie of a railway vehicle. The aim of this contribution is the bogie motion analysis with consideration of creep force effects. The comparison of the free bogie motion with the bogie motion suspended in the vehicle case is made. The solution is made for motion on the straight railway and constant forward velocity. The railway bogie is considered as perfectly rigid body which is suspended by immaterial suspension elements to the infinitely stiffness railway and vehicle case. The railway and vehicle case is considered with no degrees of freedom. The suspension between the vehicle case and the bogie is modeled by spring and damper elements. The bogie linkage with the railway is realized by creep elements. The bogie is considered with two degrees of freedom which allow the lateral motion and rotation arround the vertical axis. For the free bogie motion on the straight railway the link force effects between the bogie and the vehicle case are considered as zero. This work is based on the book Garg & Dukkipati (1984) and it follows up with the papers Švígler & Siegl (2007) and Siegl J. & Švígler J. (2006). The railway vehicle with designed velocity 200 [kmh^{-1}] is considered. The contact between the wheel sets and the railway is solved as the contact of two conical surfaces with two lines. The stiffness of rail with the subsoil is considered as infinite. The publications Jandora (2007), Moravčík & Zelenka (2007) and Byrtus, Zeman, Hlaváč (2007) dealing with the modelling and dynamical analysis

[*] Ing. Jaroslav Siegl: Faculty of Applied Sciences, Department of Mechanics, University of West Bohemia; Univerzitní 22; 301 00 Plzeň; tel.: +420 377 632 381; e-mail: jsiegl@kme.zcu.cz

[**] Doc. Ing. Jaromír Švígler, CSc.: Faculty of Applied Sciences, Department of Mechanics, University of West Bohemia; Univerzitní 22; 301 0 Plzeň; tel.: +420 377 632 304; e-mail: svigler@kme.zcu.cz

of a railway vehicle was studied.

2. Assupmtions

Vehicle suspension systems should by accurately modeled by equivalent suspension elements. In most cases for passanger and locomotive trucks, suspension characteristics can be represented by linear suspension elements. On the other hand, for most freight trucks, suspension characteristics are quite nonlinear and therefore they are required to be modeled by nonlinear elements. In developing the equations of motion for the railway vehicle model, the following assumptions are made. The vehicle frame is assumed to be rigid and its stiffness is lumped in the suspension elements. The wheel sets are assumed to run freely in the journal bearings without bearing friction, all displacements in suspension elements are considered to be small, nonlinearities due to suspension stops, wheel–flange contact, dry friction in suspension elements and adhesion limits between wheel and rail are neglected. The simpified wheel and rail contact geometry and linear creep theory is used, the gyroscope moments of wheel sets are neglected, there is no wheel lift and the wheels are always in contact with the rails.

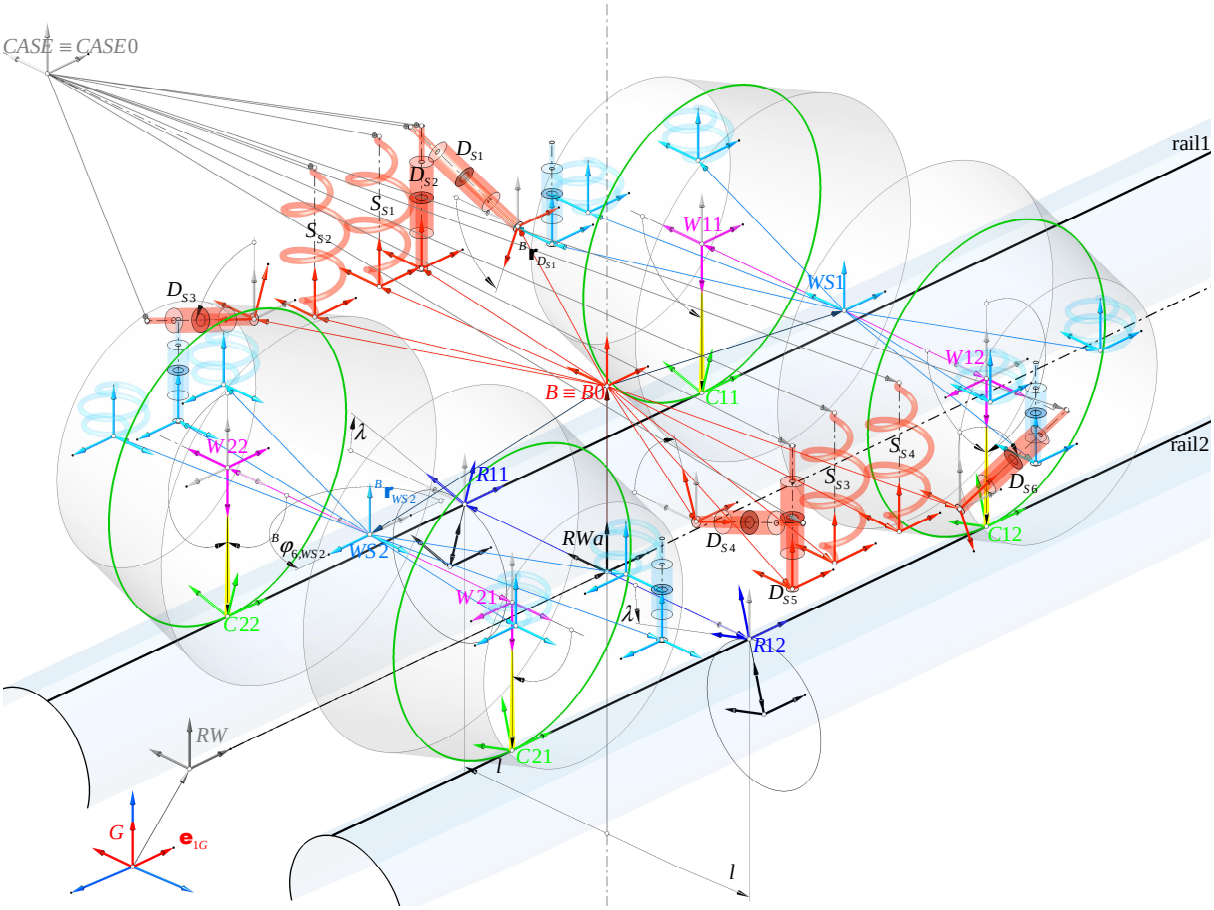

Fig. 1: General view on the bogie in default position – coordinate systems.

3. Used mathematical style

A generalized coordinate vector of a coordinate system *b* expressed in a coordinate system *a* has the form ${}^a\mathbf{q}_b = \left[{}^a\bar{\mathbf{r}}_b^T \quad {}^a\bar{\boldsymbol{\varphi}}_b^T \right]^T \in \mathbb{R}^6$ where ${}^a\bar{\mathbf{r}}_b$, ${}^a\bar{\boldsymbol{\varphi}}_b \in \mathbb{R}^3$ is a linear and an angular coordi-

nate, the ${}^{a}\mathbf{r}_b = \left[{}^{a}\bar{\mathbf{r}}_b^T \quad 1 \right]^T$, ${}^{a}\boldsymbol{\varphi}_b = \left[{}^{a}\bar{\boldsymbol{\varphi}}_b^T \quad 0 \right] \in \mathbb{R}^4$ is a linear and an angular extended coordinate. The left upper index means generaly a name of a coordinate system in which a given magnitude is expressed. A transformation matrix ${}^{a,b}\mathbf{T} \in \mathbb{R}^{4\times4}$ determines a coordinate system *b* expressed in a coordinate system *a*, the $\mathbf{T}_R \in \mathbb{R}^{3\times3}$ indicates a rotary transformation matrix. The work uses right-handed Cartesian coordinate systems whose the first base vectors on all figures are marked by black dots at the vertex of a vector conus.

4. Input parameters

It is considered a biaxial bogie of an electric locomotive that does not generates neither tractive nor braking force effects. A revolving pin, a part of secondary springs and dampers have to be considered as a component of a locomotive case. The weight of these parts is in total 523 [*kg*]. The mass inertia moments are expressed to the mass centers always. For simplification the generalized coordinate of the bogie mass center from the bogie equilibrium or default position ${}^{B0}\mathbf{q}_B(t)$ with two degrees of freedom is marked as

$$\mathbf{q}(t) = \begin{bmatrix} 0 & y & 0 & 0 & 0 & \psi \end{bmatrix}^T. \tag{1}$$

Hence the longitudinal motion performs the railway, the vertical, roll and pitch motion of the bogie is not considered. The *roll*, *pitch* and *yaw* angles constitute rotation around the *i*-th base vector of the bogie coordinate system *B* in the equilibrium position ${}^{RWa}\mathbf{e}_{iB0}$.

4.1. Wheel–Rail common parameters

The half of the rail gauge is l = 750 [*mm*], the half vertex angle of the the cone wheel is $\lambda = \operatorname{atan}(1/20)$ and the coefficient of static dry friction between the rail and the wheel is considered f_{RW} = 0,4 [–].

4.2. Railway

The bogie motion is assumed on the the first straight railway segment only which is described in the fixed coordinate system *RW*, Fig. 1. This system is placed in the global coordinate system *G* by the coordinate ${}^{G}\mathbf{q}_{RW} = \begin{bmatrix} 100 & 0 & 300 & 0 & 0 & 0 \end{bmatrix}^T$. The moveable system *RWa* is defined by the coordinate ${}^{RW}\mathbf{q}_{RWa} = \begin{bmatrix} u_{RW} & 0 & 0 & 0 & 0 & 0 \end{bmatrix}^T$ where the parameter $u_{RW} \in \langle 0, L \rangle$ is the coordinate on the railway segment, the L is the railway length and $u_{RW} = vt$ where v is forward velocity and t is the time coordinate. This *RWa*, active coordinate system, actualy defines or draws the railway curve.

4.2.1. Rail

The rail has material properties Young's rigidity modulus at pull E_R = 210 000 [*MPa*] and Poisson's ratio v_R = 0,25 [–], geometrical parameters are the principal normal radiuses of curvatures at the default contact point $\mathbf{R}_R = \begin{bmatrix} \infty & 300 \end{bmatrix}^T$ [*mm*] where the first radius of curvature R_{R1} is expressed in the longitudinal and the second one R_{R2} in the lateral direction. The coordinates matrix of the rails *R*1*j* at each railway segment is, Fig. 1,

${}^{RWa}\mathbf{q}_{R1} = \left[{}^{RWa}\mathbf{q}_{R1j} \right] = diag\left(\begin{bmatrix} 0 & l & 0 & \lambda & 0 & 0 \end{bmatrix} \right) \begin{bmatrix} 0 & 1 & 0 & 1 & 0 & 0 \\ 0 & -1 & 0 & -1 & 0 & 0 \end{bmatrix}^T$. The *j*-th rail is conside-

red as a curve, which is given by following vector function in global coordinate system *G*

$$ {}^{G}\mathbf{r}_{Rj}\left(u_{RW}\right) = {}^{G,RW}\mathbf{T}\,{}^{RW,RWa}\mathbf{T}\left(u_{RW}\right){}^{RWa,R1j}\mathbf{T}\left[0 \quad 0 \quad 0 \quad 1\right]^{T}. \tag{2} $$

4.3. Parameters of the whole bogie

The bogie contain two wheel sets which have two degrees of freedom, vertical and roll freedom, however these wheelsets are rigidly connected to the bogie in every point of time. The whole bogie is therefore considered as a rigid body. The bogie weight is m_B = 15 760 [*kg*], the mass inertia tensor in the bogie coordinate system *B* is

$${}^{B}\mathbf{I}_{B} = \begin{bmatrix} 16\,062{,}721 & -207{,}752 & -1{,}318 \\ -207{,}752 & 26\,375{,}833 & -3{,}474 \\ -1{,}318 & -3{,}474 & 24\,232{,}248 \end{bmatrix} \left[kgm^{2}\right]$$ and the coordinate of the bogie mass center in the equilibrium, default position, is ${}^{RWa}\mathbf{q}_{B0} = \left[0 \quad 0 \quad 727 \quad 0 \quad 0 \quad 0\right]^{T}$ [*mm*]. The coordinates matrix of the *i*-th wheel set in the equilibrium position in the bogie coordinate system *B* is ${}^{B}\mathbf{q}_{WS0} = \left[{}^{B}\mathbf{q}_{WS0i}\right] = \begin{bmatrix} 1\,250 & 0 & -102 & 0 & 0 & 0 \\ -1\,250 & 0 & -102 & 0 & 0 & \pi \end{bmatrix}^{T}$, the coordinates matrix of the *j*-th wheel on the *i*-th wheel set at the *i*-th wheel set coordinate system *WSi* is

$${}^{WSi}\mathbf{q}_{W} = \left[{}^{WSi}\mathbf{q}_{Wij}\right] = \begin{bmatrix} 0 & l & 0 & -0{,}5\pi & 0 & 0 \\ 0 & -l & 0 & 0{,}5\pi & \pi & 0 \end{bmatrix}^{T}.$$

4.3.1. Wheel

The wheel has material properties Young's rigidity modulus at pull E_W = 210 000 [*MPa*] and Poisson's ratio ν_W = 0,25 [–], the geometrical parameters, principal normal radiuses of curvatures at the default contact point, are approximatelly considered

$\mathbf{R}_W = \left[1\,250/2 \quad 100\,000\right]^{T}$ [*mm*] where the first radius of curvature R_{W1} is in the longitudinal and the second one R_{W2} in the lateral direction. The coordinates matrix of the wheels *Wij* on the *i*-th wheel set *WSi* is, Fig. 1,

${}^{WS}\mathbf{q}_{W} = \left[{}^{WSi}\mathbf{q}_{Wij}\right] = \begin{bmatrix} 0 & l & 0 & -0{,}5\pi & 0 & 0 \\ 0 & -l & 0 & 0{,}5\pi & \pi & 0 \end{bmatrix}^{T}$. The wheel rolling surface is considered as a conical surface, which is described by following vector function in the actual coordinate system

$$ \mathbf{r}_{W}\left(u_1,\, u_2\right) = \begin{bmatrix} \left(R_{W1} - u_1 \tan\lambda\right)\cos u_2 \\ \left(R_{W1} - u_1 \tan\lambda\right)\sin u_2 \\ u_1 \\ 1 \end{bmatrix} \tag{3} $$

where u_1, u_2 are surface parameters. The *j*-th wheel surface of the *i*-th wheel set in the global coordinate system is given

$$ {}^{G}\mathbf{r}_{Wij}\left(u_1,\, u_2\right) = {}^{G,RW}\mathbf{T}\,{}^{RW,RWa}\mathbf{T}\left(u_{RW}\right){}^{RWa,B0}\mathbf{T}\,{}^{B0,B}\mathbf{T}\,{}^{B,WS0i}\mathbf{T}\,{}^{WS0i,WSi}\mathbf{T}\left({}^{WS0i}\mathbf{q}_{WSi}\right){}^{WSi,Wij}\mathbf{T}\,{}^{Wij}\mathbf{r}_{W}\left(u_1,\, u_2\right), \tag{4} $$

tangential vectors at each wheel point

$$ {}^{G}\mathbf{t}_{1Wij}(u_1,\ u_2)=\frac{\partial\,{}^{G}\mathbf{r}_{Wij}}{\partial u_1}=\begin{bmatrix}-\tan\lambda\cos u_2\\ -\tan\lambda\sin u_2\\ 1\\ 0\end{bmatrix},\quad {}^{G}\mathbf{t}_{2Wij}(u_1,\ u_2)=\frac{\partial\,{}^{G}\mathbf{r}_{Wij}}{\partial u_2}=\begin{bmatrix}-(R_{W1}-u_1\tan\lambda)\sin u_2\\ (R_{W1}-u_1\tan\lambda)\cos u_2\\ 0\\ 0\end{bmatrix} \tag{5} $$

and the normal vector

$$ {}^{G}\bar{\mathbf{n}}_{Wij}(u_1,\ u_2)={}^{G}\bar{\mathbf{t}}_{1Wij}\times{}^{G}\bar{\mathbf{t}}_{2Wij}\,. \tag{6} $$

4.3.2. Link elements to the case – secondary suspension

The whole link elements are considered as immaterial.

Springs

There are condsidered four linear spiral springs whose high in free state is 630 [*mm*], diameter is 240 [*mm*], diameter of the wire is 48 [*mm*], axial stiffness is 538 [Nmm^{-1}], radial stiffness for static load, in accordance with Ponomarev, is 266 [Nmm^{-1}] and number of effective threads is 7. The coordinates matrix of the secondary springs coordinate systems S_{Si} is

$$ {}^{RWa}\mathbf{q}_{S_S}=\left[{}^{RWa}\mathbf{q}_{S_{Si}}\right]=diag\left(\left[170\quad 1\,370\quad 617\quad \mathbf{0}_3^T\right]\right)\begin{bmatrix}1&-1&-1&1\\ 1&1&-1&-1\\ 1&1&1&1\\ \mathbf{0}_3&\mathbf{0}_3&\mathbf{0}_3&\mathbf{0}_3\end{bmatrix},\quad i\in\{1,\ ...,\ 4\}, $$

and the matrix of the stiffness vectors is

$$ {}^{S_{Si}}\mathbf{k}_{S_S}=\left[{}^{S_{Si}}\mathbf{k}_{S_{Si}}\right]=diag\left(\left[266\quad 266\quad 538\right]\right)\begin{bmatrix}1&1&1&1\\ 1&1&1&1\\ 1&1&1&1\end{bmatrix}\left[\frac{N}{mm}\right],\quad i\in\{1,\ ...,\ 4\}\,. $$

Dampers

The whole dampers of the company KONI are modeled as linear except the longitudinal. The damping force $F^{*}_{DS,lo}$ of this longitudinal damper or *yaw damper* is given as a discrete function that is interpolated to the continuous function $F_{DS,lo}$ by the *Piecewise cubic Hermite interpolating Polynomial*, Fig. 2. This interpolation method has no overshoots and less oscillation if the data are not smooth.

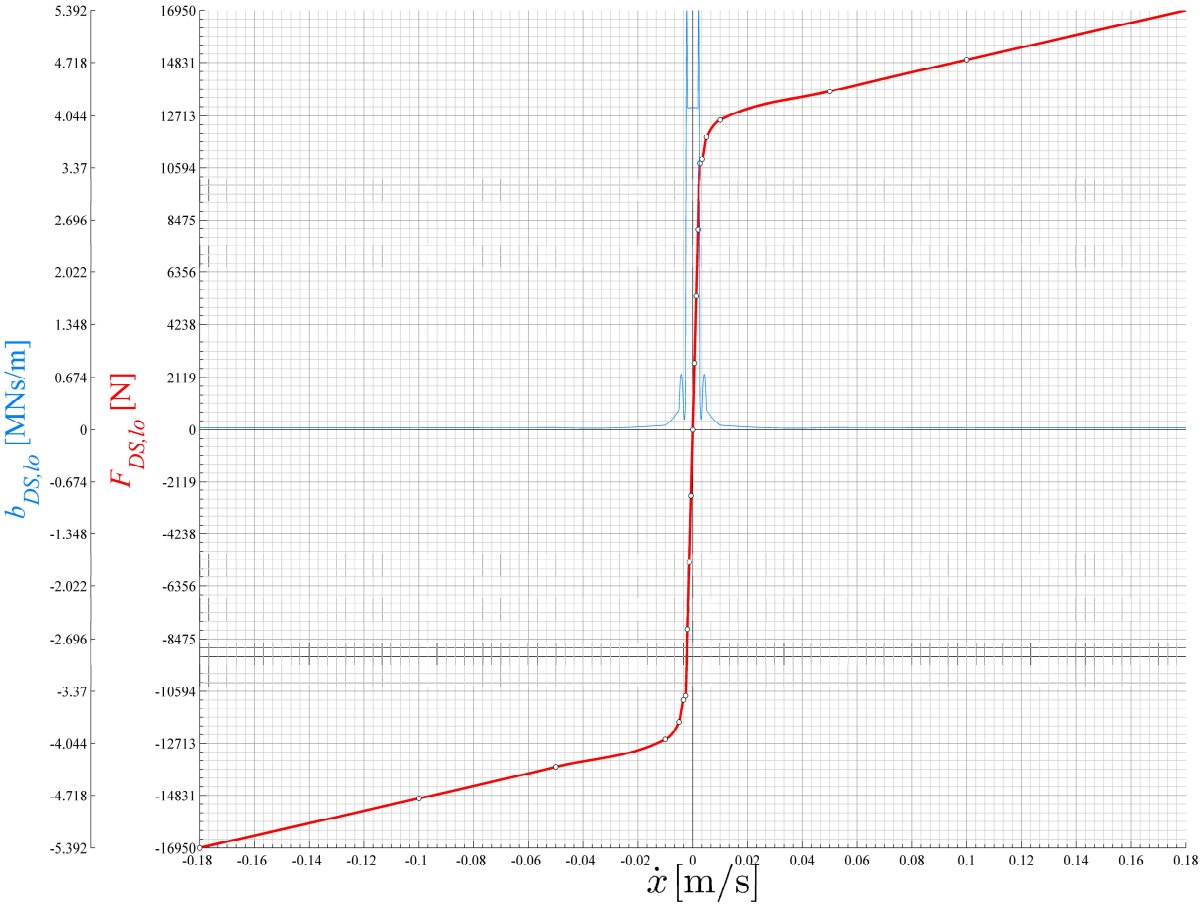

Fig. 2: Functions of longitudinal damper for secondary suspension – continuous damping force $F_{DS,lo} = F_{DS,lo}(\dot{x})$, discrete damping force $F^*_{DS,lo} = F^*_{DS,lo}(\dot{x})$ (white points) and damping $b_{DS,lo} = b_{DS,lo}(\dot{x}) = \partial F_{DS,lo} / \partial \dot{x}$ (blue curve).

The coordinates matrix of secondary dampers actual coordinate systems D_{Si} is

$$ {}^{RWa}\mathbf{q}_{D_S} = \left[{}^{RWa}\mathbf{q}_{D_{Si}} \right] =$$

$$= \left[\begin{array}{cccccc}
590 & 405 & -400 & -590 & -405 & 400 \\
1\,060 & 1\,370+12 & 1\,460 & -1\,060 & -(1\,370+12) & -1\,460 \\
885-395\tan\left(8\frac{\pi}{180}\right) & 600 & 661 & 885-395\tan\left(8\frac{\pi}{180}\right) & 600 & 661 \\
\hline
-\frac{\pi}{2}+8\frac{\pi}{180} & 0 & 0 & \frac{\pi}{2}-8\frac{\pi}{180} & 0 & 0 \\
0 & 0 & -\frac{\pi}{2}+8\frac{\pi}{180} & 0 & 0 & \frac{\pi}{2}-8\frac{\pi}{180} \\
0 & 0 & 0 & 0 & 0 & 0 \\
\textit{lateral} & \textit{vertical} & \textit{longitudinal} & \textit{lateral} & \textit{vertical} & \textit{longitudinal}
\end{array}\right]$$

$i \in \{1, \ldots, 6\}$.

and the matrix of damping vectors is

$$\mathbf{b}_{D_S} = \left[\mathbf{b}_{D_{Si}}\left({}^{B0}\dot{\mathbf{q}}_B\right)\right] =$$

$$= \left[\begin{array}{ccc|ccc} 0 & 0 & 0 & 0 & 0 & 0 \\ 0 & 0 & 0 & 0 & 0 & 0 \\ \underbrace{63\,000}_{lateral} & \underbrace{100\,000}_{vertical} & \underbrace{b_{D_{S,lo}}\left({}^{B0}\dot{\mathbf{r}}_{D_{S3}}\right)}_{longitudinal} & \underbrace{63\,000}_{lateral} & \underbrace{100\,000}_{vertical} & \underbrace{b_{D_{S,lo}}\left({}^{B0}\dot{\mathbf{r}}_{D_{S6}}\right)}_{longitudinal} \end{array}\right] \left[\frac{Ns}{m}\right]$$

where

$$ {}^{B0}\dot{\mathbf{r}}_{D_{Si}}\left({}^{B0}\dot{\mathbf{q}}_B\right) = \frac{d\left({}^{B0,B}\mathbf{T}\,{}^{B}\mathbf{r}_{D_{Si}}\right)}{dt} = {}^{B0,B}\dot{\mathbf{T}}\,{}^{B}\mathbf{r}_{D_{Si}} + \underbrace{{}^{B0,B}\mathbf{T}\,{}^{B}\dot{\mathbf{r}}_{D_{Si}}}_{0} = \left[\begin{array}{cc} {}^{B0}\boldsymbol{\Omega}_B\,{}^{B0,B}\mathbf{T}_R & {}^{B0}\dot{\overline{\mathbf{r}}}_B \\ \mathbf{0}_3^T & 0 \end{array}\right]\left[\begin{array}{c} {}^{B}\overline{\mathbf{r}}_{D_{Si}} \\ 1 \end{array}\right] = $$

$$= \left[\begin{array}{c} {}^{B0}\boldsymbol{\Omega}_B\,{}^{B0,B}\mathbf{T}_R\,{}^{B}\overline{\mathbf{r}}_{D_{Si}} + {}^{B0}\dot{\overline{\mathbf{r}}}_B \\ 0 \end{array}\right] \tag{7}$$

is the velocity vector expressed in the bogie equilibrium position *B*0 of the *i*-th damper and the ${}^{B0}\boldsymbol{\Omega}_B$ is the bogie angular velocity in the matrix form.

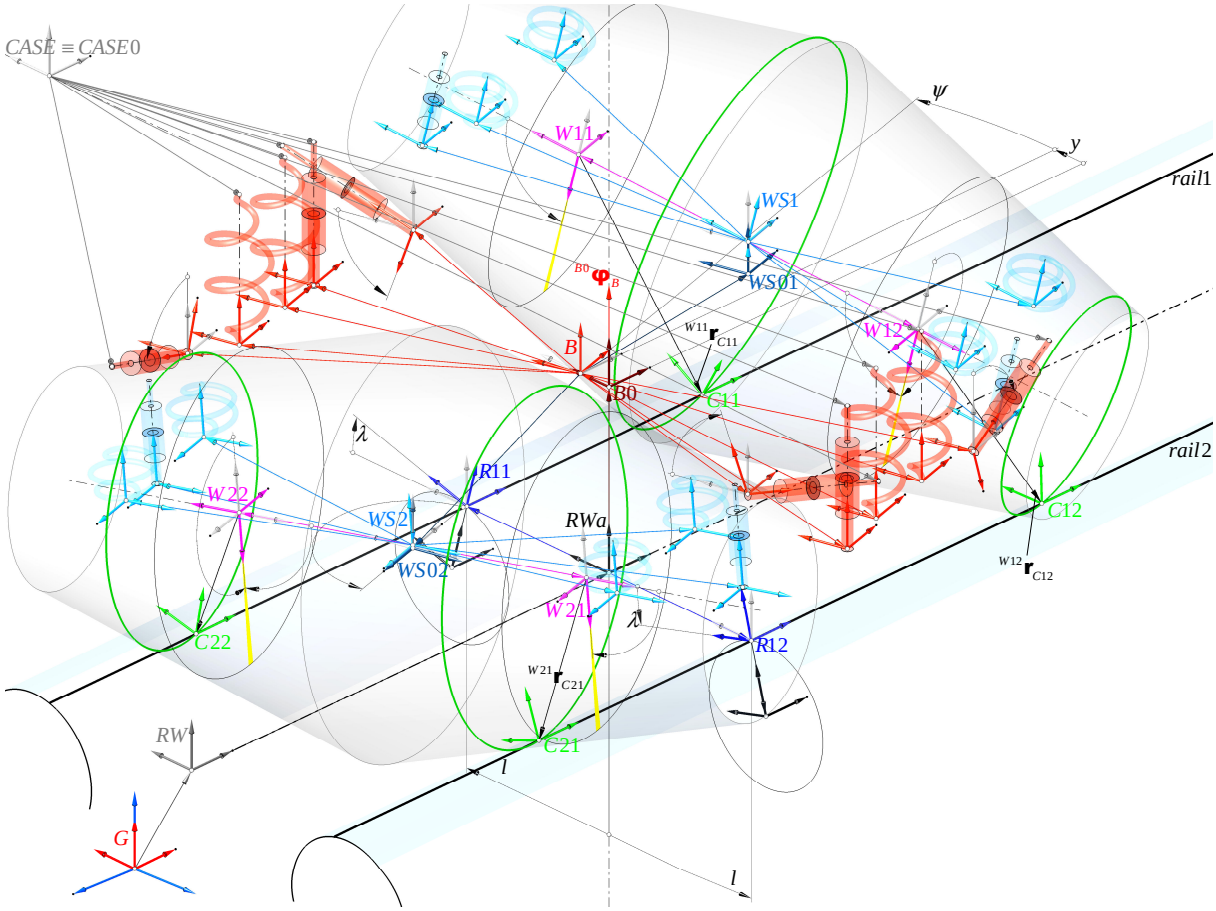

Fig. 3: General view on the bogie in a general position.

4.4. Case of locomotive

To the case of vehicle is added mass of the rotary pin and upper part of the secondary suspension. The case weight is m_{CASE} = 55 526 [*kg*], the mass inertia tensor is

${}^{CASE}\mathbf{I}_{CASE} = diag\left([104\ 772 \quad 1\ 037\ 305 \quad 1\ 037\ 091]\right)\ \left[kgm^2\right]$ and the coordinate of the case mass center in the equilibrium position is ${}^{RWa}\mathbf{q}_{CASE0} = [-3200 \quad 0 \quad 1\ 713 \quad 0 \quad 0 \quad 0]^T$. The case is considered with no degree of freedom, hence ${}^{CASE0}\mathbf{q}_{CASE} = \mathbf{0}_6$.

5. Analysis

The bogie suspension system is modeled by *nonlinear suspension elements*. The bogie is modeled as a discrete mechanical system, thus on condition of perfectly rigid bodies which are linked by immaterial linkages.

5.1. Bogie constrains

The wheel sets, which are rigidly connected to the bogie, are constrained by the rails which take away three degrees of freedom. The wheel set pitch freedom is not considered. The *i*-th wheel set coordinate is so

$${}^{WS0i}\mathbf{q}_{WSi} = \left[0 \quad 0 \quad {}^{WS0i}z_{WSi} \quad {}^{WS0i}\phi_{WSi} \quad 0 \quad 0\right]^T . \tag{8}$$

The wheel set – rails contact is solved simpli as *biconus on two parallel lines*. The conditions of the *i*-th wheel set – rails contact are following

$$\begin{aligned} {}^{G}\mathbf{r}_{R1} - {}^{G}\mathbf{r}_{Wi1} &= \mathbf{0}_4, \\ {}^{G}\mathbf{t}_{R1}^{T}\ {}^{G}\mathbf{n}_{Wi1} &= 0, \\ {}^{G}\mathbf{r}_{R2} - {}^{G}\mathbf{r}_{Wi2} &= \mathbf{0}_4, \\ {}^{G}\mathbf{t}_{R2}^{T}\ {}^{G}\mathbf{n}_{Wi2} &= 0 \end{aligned} \tag{9}$$

where ${}^{G}\mathbf{t}_{Rj}$ is tangential vector of the *j*-th rail curve. These eight non-linear equations $\mathbf{F}(\mathbf{x}) = \mathbf{0}$ solves the unknow vector

$$\mathbf{x} = \left[u_{RW1} \quad u_{1W1} \quad u_{2W1} \mid u_{RW2} \quad u_{1W2} \quad u_{2W2} \mid {}^{WS0i}z_{WSi} \quad {}^{WS0i}\phi_{WSi}\right]^T \in \mathbb{R}^8 . \tag{10}$$

The Fig. 3 is generated with application of this contact detection method.

6. Motion equation

The condition of the bogie dynamic equilibrium in the bogie coordinate system *B* is in the vector form

$${}^{B}\mathbf{Q}_I(\ddot{\mathbf{q}}) + {}^{B}\mathbf{Q}_D(\dot{\mathbf{q}}) + {}^{B}\mathbf{Q}_S(\mathbf{q}) + {}^{B}\mathbf{Q}_C(\mathbf{q},\dot{\mathbf{q}}) + {}^{B}\mathbf{Q}_A(\mathbf{q}) + {}^{B}\mathbf{Q}_R(\mathbf{q}) = \mathbf{0}_6 \tag{11}$$

where $\mathbf{Q}_I$ is an inertia force effect of the bogie, $\mathbf{Q}_D$ is a dissipative force effect of damper elements, $\mathbf{Q}_S$ is a force effect of spring elements, $\mathbf{Q}_C$ is a force effect of creep elements and $\mathbf{Q}_A$, $\mathbf{Q}_R$ is the gravity action and reactive force effect. The coordinate of the *i*-th linkage element in the bogie coordinate system *B* is

$${}^{RWa}\mathbf{r}_i = {}^{RWa,B0}\mathbf{T}\left({}^{RWa}\mathbf{q}_{B0}\right){}^{B0}\mathbf{r}_i \quad \Rightarrow \quad {}^{B0}\mathbf{r}_i = {}^{B}\mathbf{r}_i = inv\left({}^{RWa,B0}\mathbf{T}\right){}^{RWa}\mathbf{r}_i . \tag{12}$$

6.1. Inertia force effect

The inertia force effect is expressed

$$ {}^{B}\mathbf{Q}_{I} = -\mathbf{M}\ddot{\mathbf{q}}, \qquad \mathbf{M} = \begin{bmatrix} m_{B}\mathbf{E} & \mathbf{0} \\ \mathbf{0} & {}^{B}\mathbf{I}_{B} \end{bmatrix} \tag{13} $$

where $\mathbf{M} \in \mathbb{R}^{6\times 6}$ is the *mass matrix* of the bogie and $\mathbf{E} \in \mathbb{R}^{3\times 3}$ is the identity matrix.

6.2. Damper force effect

The force effect of the damper elements is expressed

$$ {}^{B}\mathbf{Q}_{D} = -\mathbf{B}(\dot{\mathbf{q}})\dot{\mathbf{q}}, \qquad \mathbf{B} = \mathbf{B}(\dot{\mathbf{q}}) = \sum_{i=1}^{6} \left[\begin{array}{c|c} {}^{B}\mathbf{B}_{D_{Si}} & {}^{B}\mathbf{B}_{D_{Si}}\,{}^{B}\mathbf{R}_{D_{Si}}^{T} \\ \hline {}^{B}\mathbf{R}_{D_{Si}}\,{}^{B}\mathbf{B}_{D_{Si}} & {}^{B}\mathbf{R}_{D_{Si}}\,{}^{B}\mathbf{B}_{D_{Si}}\,{}^{B}\mathbf{R}_{D_{Si}}^{T} \end{array} \right] \tag{14} $$

where $\mathbf{B} \in \mathbb{R}^{6\times 6}$ is the *damping matrix* of the bogie, ${}^{B}\mathbf{R}_{D_{Si}}$ is the position vector in matrix form of the *i*-th secondary damper in the bogie coordinate system and ${}^{B}\mathbf{B}_{D_{Si}} \in \mathbb{R}^{3\times 3}$ is the transformated damping matrix of the *i*-th secondary damper which is given by

$$ {}^{B}\mathbf{B}_{D_{Si}} = {}^{\bar{B},D_{Si}}\mathbf{T}_{R}\left({}^{B}\boldsymbol{\varphi}_{D_{Si}}\right) {}^{D_{Si}}\mathbf{B}_{D_{Si}}\, {}^{\bar{B},D_{Si}}\mathbf{T}_{R}^{T}\left({}^{B}\boldsymbol{\varphi}_{D_{Si}}\right) \tag{15} $$

where the coordinate system $\bar{B}$ is parallel with the coordinate system *B*. The damping matrix has the form ${}^{D_{Si}}\mathbf{B}_{D_{Si}} = diag\left(\mathbf{b}_{D_{Si}}\right)$.

6.3. Spring force effect

The force effect of the spring elements is expressed

$$ {}^{B}\mathbf{Q}_{S} = -\mathbf{K}\mathbf{q}, \qquad \mathbf{K} = \sum_{i=1}^{4} \left[\begin{array}{c|c} {}^{B}\mathbf{K}_{S_{Si}} & {}^{B}\mathbf{K}_{S_{Si}}\,{}^{B}\mathbf{R}_{S_{Si}}^{T} \\ \hline {}^{B}\mathbf{R}_{S_{Si}}\,{}^{B}\mathbf{K}_{S_{Si}} & {}^{B}\mathbf{R}_{S_{Si}}\,{}^{B}\mathbf{K}_{S_{Si}}\,{}^{B}\mathbf{R}_{S_{Si}}^{T} \end{array} \right] \tag{16} $$

where $\mathbf{K} \in \mathbb{R}^{6\times 6}$ is the *stiffness matrix* of the bogie, ${}^{B}\mathbf{R}_{S_{Si}}$ is the position vector in matrix form of the *i*-th secondary spring in the bogie coordinate system *B* and ${}^{B}\mathbf{K}_{S_{Si}} \in \mathbb{R}^{3\times 3}$ is the transformated damping matrix of the *i*-th secondary spring which is given by

$$ {}^{B}\mathbf{K}_{D_{Si}} = {}^{\bar{B},S_{Si}}\mathbf{T}_{R}\left({}^{B}\boldsymbol{\varphi}_{S_{Si}}\right) {}^{S_{Si}}\mathbf{K}_{S_{Si}}\, {}^{\bar{B},S_{Si}}\mathbf{T}_{R}^{T}\left({}^{B}\boldsymbol{\varphi}_{S_{Si}}\right). \tag{17} $$

The *i*-th spring actual coordinate system S_{Si} lies in the *principal central axes of elasticity* (PCAE). The spring is sometimes called as the *elastic insulator*. The stiffness matrix has the form ${}^{S_{Si}}\mathbf{K}_{S_{Si}} = diag\left(\mathbf{k}_{S_{Si}}\right)$.

6.4. Gravity force effects

The action force effect on the bogie is caused by the gravitational field only with acceleration *g* and therefore

$$ {}^{B}\mathbf{Q}_{A} = \begin{bmatrix} 0 & 0 & -\left(m_{B} + 0{,}5m_{CASE}\right)g & 0 & 0 & 0 \end{bmatrix}^{T}. \tag{18} $$

On the *i*-th wheel set it affects

$$ {}^{WSi}\mathbf{Q}_A = \begin{bmatrix} 0 & 0 & -\left(m_B + 0{,}5m_{CASE}\right) g/2 & 0 & 0 & 0 \end{bmatrix}^T . \tag{19} $$

This action force effect causes the reactive force effects at the wheel-rail contacts of the *i*-th wheel set for the static equilibrium. These reactive force effects are given by the condition of the static equilibrium

$$ {}^{WSi}\mathbf{Q}_A + \sum_{j=1}^{2} \left\{ \left[\begin{array}{c|c} {}^{\overline{Cij},\,Cij}\mathbf{T}_R & \mathbf{0}_{3\times 3} \\ \hline {}^{WSi}\mathbf{R}_{Ci}\,{}^{\overline{Cij},\,Cij}\mathbf{T}_R & {}^{\overline{Cij},\,Cij}\mathbf{T}_R \end{array} \right] {}^{Cij}\mathbf{Q}_R \right\} = \mathbf{0}_6 \tag{20} $$

where the reactive force at the contact *Cij* has the form ${}^{Cij}\mathbf{Q}_R = \begin{bmatrix} F_{R1} & F_{R2} & F_{R3} & 0 & 0 & 0 \end{bmatrix}^T$. The Eq. 20 is actually a vector linear equation $\mathbf{F}(\mathbf{x}) = \mathbf{0}$ where $\mathbf{F}$ is a vector function, $\mathbf{x}$ is a vector of solution and $\mathbf{0}$ is the zero vector. The reactive forces at the contact tangential plane, F_{R1} and F_{R2}, secure the static state, but a motion on this plane is possible. Therefore the third reactive force F_{R3} only is applicated to the motion equation

$$ {}^{Cij}\mathbf{Q}_R = \begin{bmatrix} 0 & 0 & F_{R3} & 0 & 0 & 0 \end{bmatrix}^T . \tag{21} $$

This reactive force effect ${}^{Cij}\mathbf{Q}_R$ is equivalently replaced in the bogie coordinate system *B* and the result reactive force effect caused by the gravitational field is following

$$ {}^{B}\mathbf{Q}_R = \sum_{i=1}^{2}\sum_{j=1}^{2} \left\{ \left[\begin{array}{c|c} {}^{\overline{Cij},\,Cij}\mathbf{T}_R & \mathbf{0}_{3\times 3} \\ \hline {}^{B}\mathbf{R}_{Cij}\,{}^{\overline{Cij},\,Cij}\mathbf{T}_R & {}^{\overline{Cij},\,Cij}\mathbf{T}_R \end{array} \right] {}^{Cij}\mathbf{Q}_R \right\} \tag{22} $$

where the coordinate system $\overline{Cij}$ is parallel with the bogie coordinate system. The force ${}^{B}Q_{R2}$ is sometimes called the *lateral gravitational stiffness* and the moment ${}^{B}Q_{R6}$ the *yaw gravitational stiffness*. The force ${}^{Cij}\mathbf{F}_R$ in the Eq. 21 is called the *wheel force*.

6.5. Creep force effects

The creep force effect at the contact coordinate system *Cij* of the *i*-th wheel set and the *j*-th wheel, whose the third base vector is always perpendicular to the contact tangential plane, is described by the Kalker's linear theory of rolling contact, Kalker (1967). In the matrix form it is possible to express as

$$ {}^{Cij}\mathbf{Q}_C = -\mathbf{C}(\mathbf{q})\,\mathbf{g}(\mathbf{q}, \dot{\mathbf{q}}) \tag{23} $$

where $\mathbf{C}$ is a square antisymetrical matrix of the Kalker's linear functions and $\mathbf{g}$ is the creepages vector of a wheel and a rail. This equation has form

$$ {}^{Cij}\mathbf{Q}_C = \begin{bmatrix} T_x \\ T_y \\ 0 \\ 0 \\ 0 \\ M_z \end{bmatrix} = -\begin{bmatrix} (ab)^1 GC_{11} & 0 & 0 & 0 & 0 & 0 \\ & (ab)^1 GC_{22} & 0 & 0 & 0 & (ab)^{\frac{3}{2}} GC_{26} \\ & & 0 & 0 & 0 & 0 \\ & & & 0 & 0 & 0 \\ & & & & 0 & 0 \\ -sym & & & & & (ab)^2 GC_{66} \end{bmatrix} \begin{bmatrix} \gamma_1 \\ \gamma_2 \\ 0 \\ 0 \\ 0 \\ \gamma_6 \end{bmatrix} \tag{24} $$

where T_x is longitudinal creep force, T_y is lateral creep force and M_z is spin-creep moment. Linear creep force T_x is independent of γ_2 and γ_6, whereas T_y is independent of γ_1. This Kalker's theory uses the *combined elastic constants* v and G for the case of two different rolling bodies where v is combined Poisson's ratio and G is combined shear modulus of rigidity of wheel and rail. The Kalker's creep function $C_{ij} = C_{ij}(v, a/b)$ depends on the Poisson's ratio v and the ratio a/b of the semiaxes of the contact elliptical surface only. The functions C_{26} and C_{66} are marked in the publication Garg, V. K. & Dukkipati, R. V. (1984) as C_{23} and C_{33}. These Kalker's continuous creep functions C_{ij} are obtained from discrete creep function by cubic spline interpolation method, Siegl J. & Švígler J. (2006).

6.5.1. Creepages determination

Creepage occurs in all three directions in which relative motion can occur. This creepage or relative slip at the contact point *Cij* of the *i*-th wheel set and the *j*-th wheel in the *k*-th direction is defined as a quotient of the slide velocity in this direction and the forward velocity v of a vehicle generaly, hence

$$ {}^{Cij}\gamma_k = \frac{v_{slide,k}}{|v|}, \quad k \in \{1,2,6\}. \tag{25} $$

There are obtained the creepage in the longitudinal γ_1, the lateral γ_2 and the normal γ_6 direction, Siegl J. & Švígler J. (2006). The equations of Johnson and Vermeulen, Johnson K. L. & Vermeulen P. J. (1964), then modify the tangential forces because of creep force linearization, when the tangential force size can exceeds the friction force $f_{RW}\left|{}^{Cij}\mathbf{F}_R\right|$, which is unreal.

6.5.2. Equivalent replacement of creep force effects

The creep force effects are equivalently replaced in the bogie coordinate system *B* as following

$$ {}^{B}\mathbf{Q}_C = \sum_{i=1}^{2}\sum_{j=1}^{2}\left\{\left[\begin{array}{c|c} {}^{\overline{Cij},\,Cij}\mathbf{T}_R & \mathbf{0}_{3\times3} \\ \hline {}^{B}\mathbf{R}_{Cij}\,{}^{\overline{Cij},\,Cij}\mathbf{T}_R & {}^{\overline{Cij},\,Cij}\mathbf{T}_R \end{array}\right] {}^{Cij}\mathbf{Q}_C\right\} \tag{26} $$

where the coordinate system $\overline{Cij}$ is parallel with the bogie coordinate system.

7. Numerical simulation

On the following figures the functions at the left rail are ploted by green color, at the right one by blue and the first (front) wheel set by continuous, the second (back) one by dot line type. The numerical simulations are made for initial values y_0 = 0,005 [m], $\dot{y}_0$ = 0 [ms^{-1}], ψ_0 = 0 [rad], $\dot{\psi}_0 = 0$ [$rads^{-1}$].

7.1. Motion of the free bogie

On the following figures are visualized some functions of the biaxial bogie motion without secondary suspension, i.e. $\mathbf{K} = \mathbf{0}$ and $\mathbf{B} = \mathbf{0}$.

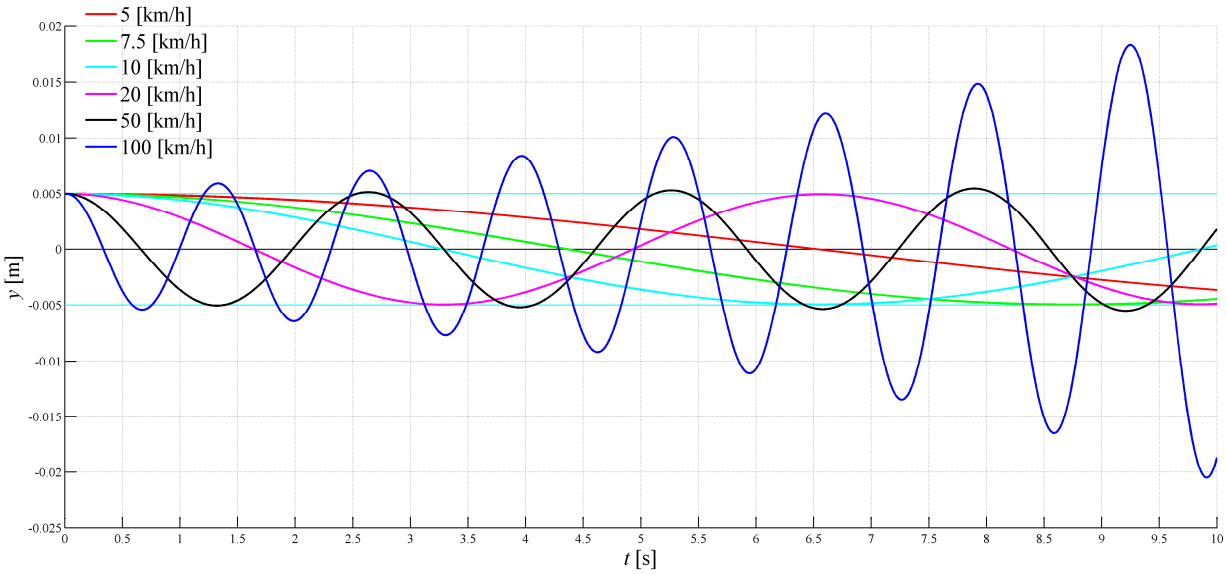

Fig. 4: Functions $y = y(t)$ describing the bogie lateral motion for selected forward velocities.

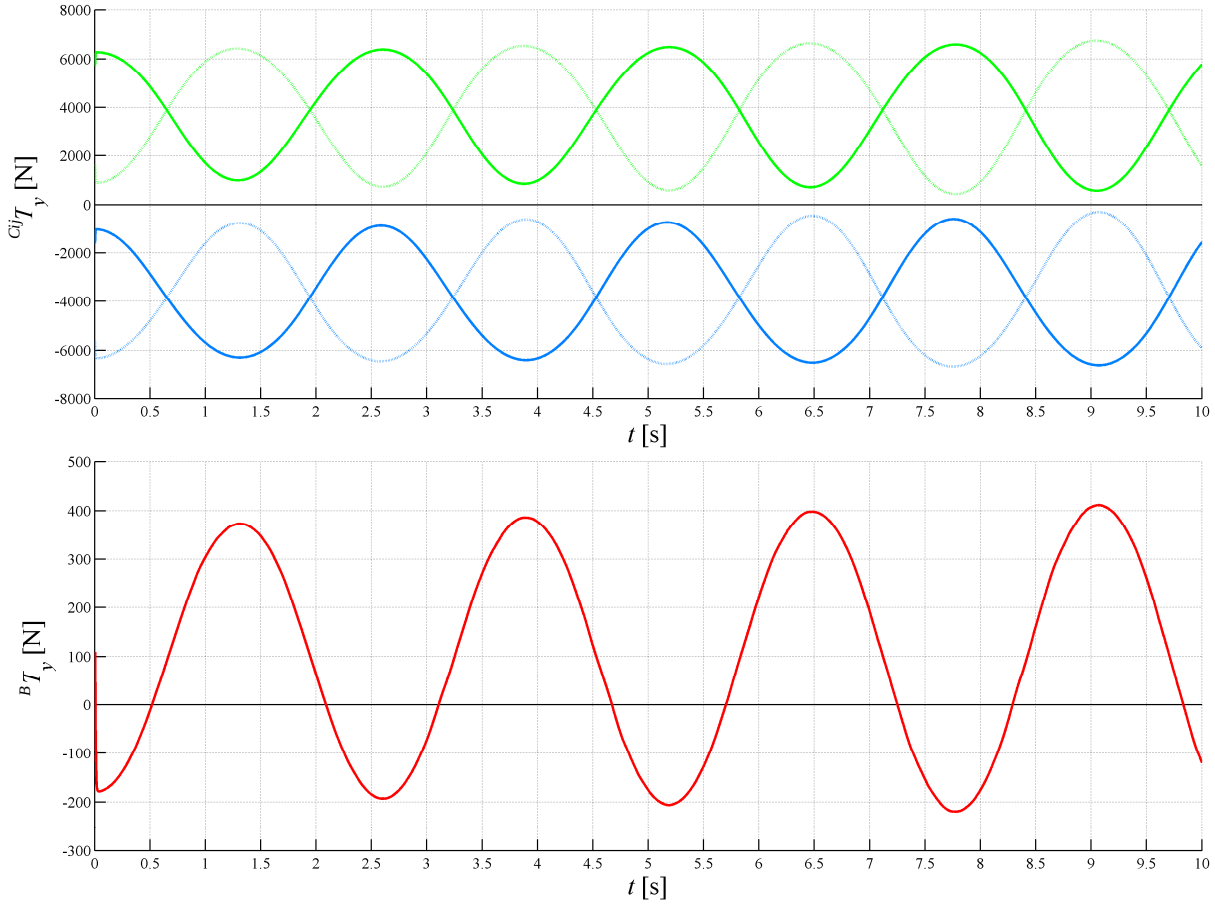

Fig. 5: Lateral creep forces and result creep force affecting the bogie motion for the forward velocity 50 [kmh^{-1}].

7.2. Motion of the suspended bogie in the vehicle case

On the following figures are visualized some functions of the biaxial bogie motion with sec-

ondary suspension. On the Fig. 8 up to the Fig. 11 the creepages and the creep force effects are ploted for the forward velocity $v = 50$ [kmh^{-1}].

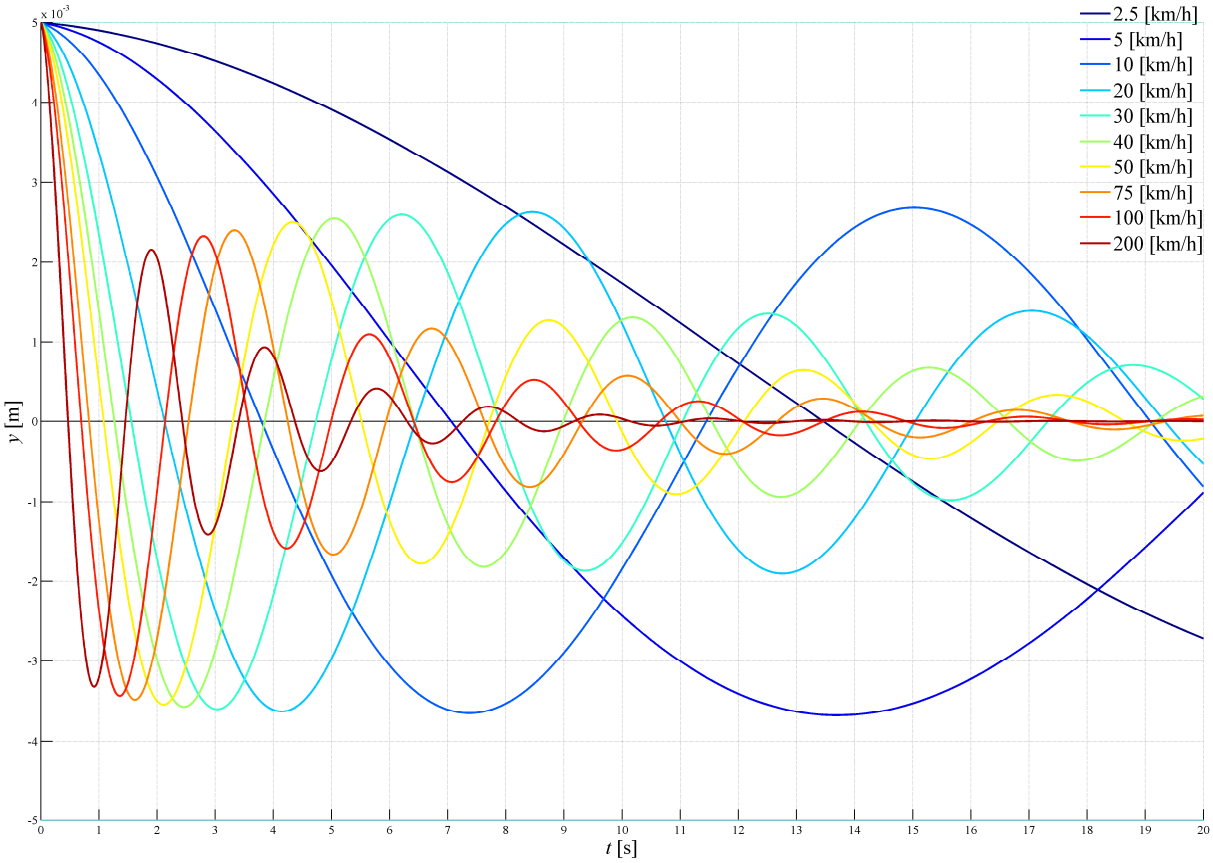

Fig. 6: Functions $y = y(t)$ describing the bogie lateral motion for selected forward velocities.

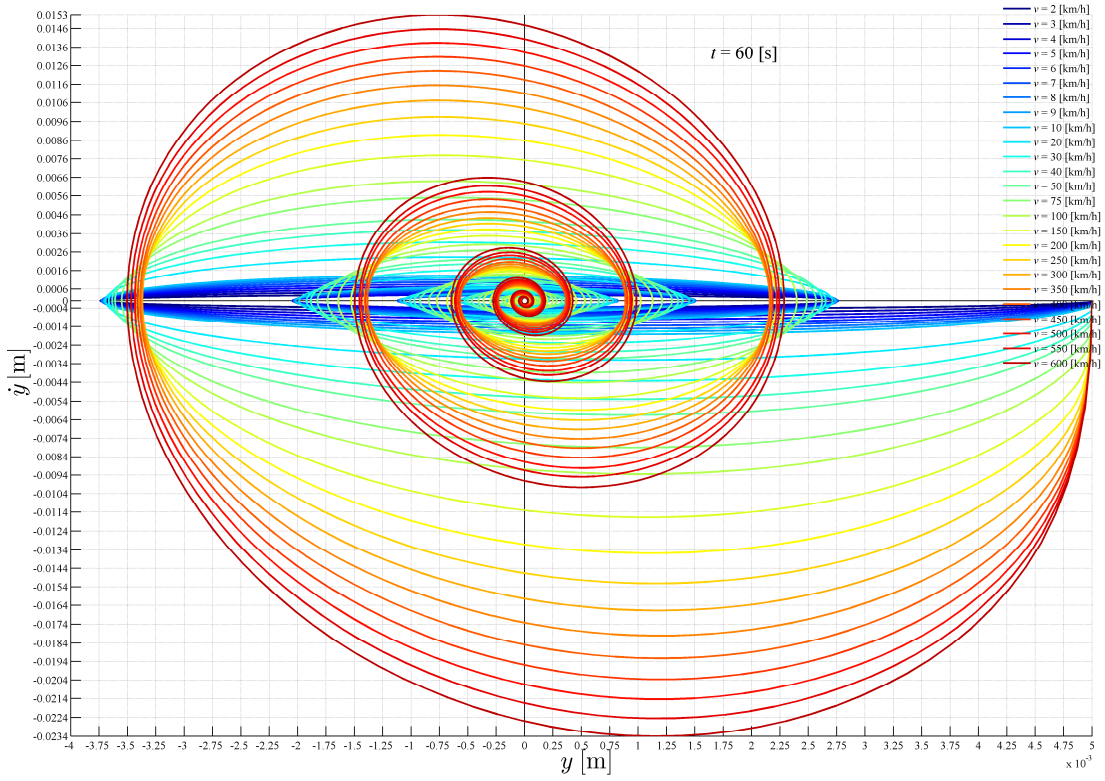

Fig. 7: Functions $\dot{y} = \dot{y}(y)$ or the *phase trajectories* for selected forward velocities *v* and motion time *t* = 60 [*s*].

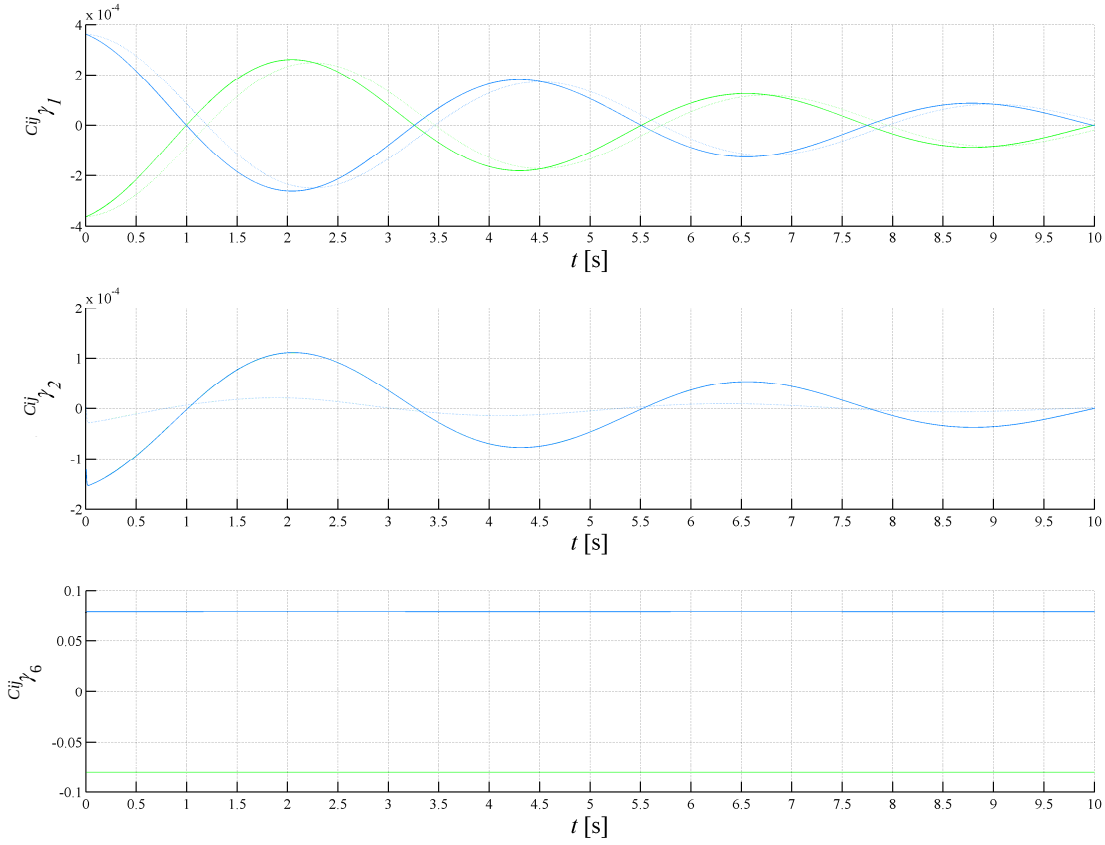

Fig. 8: Creepages γ_i.

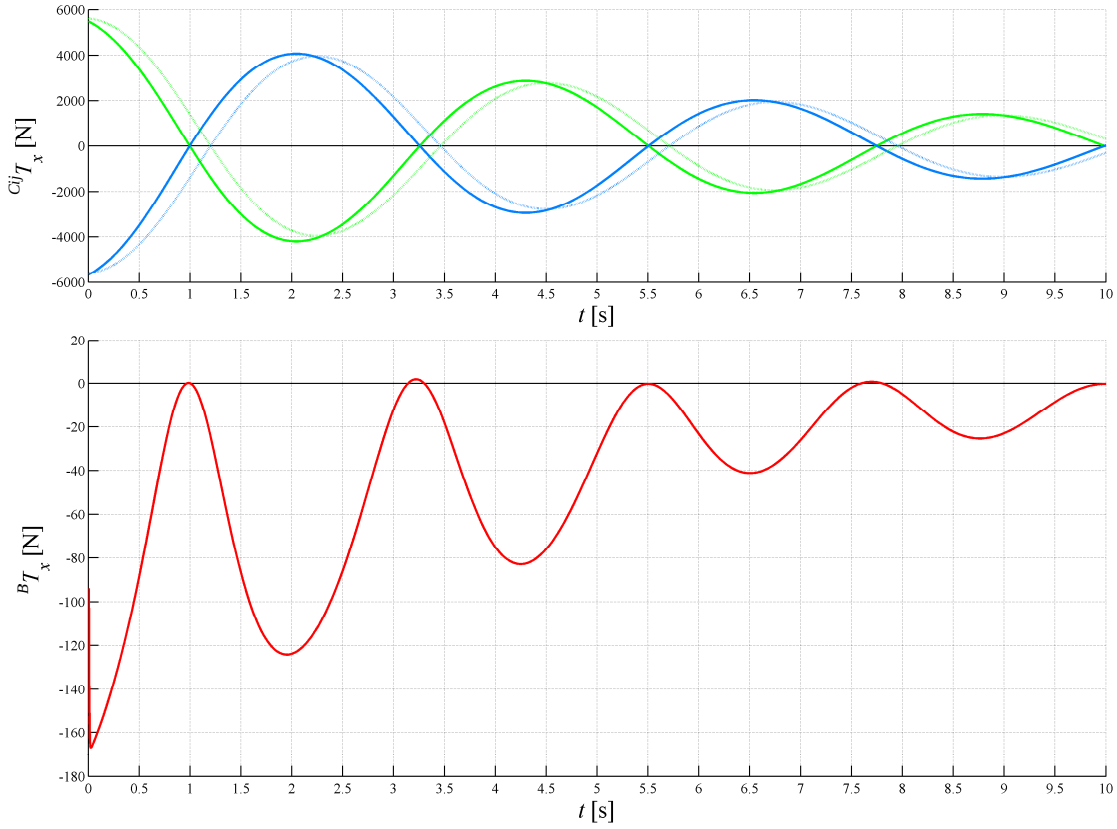

Fig. 9: Longitudinal creep forces.

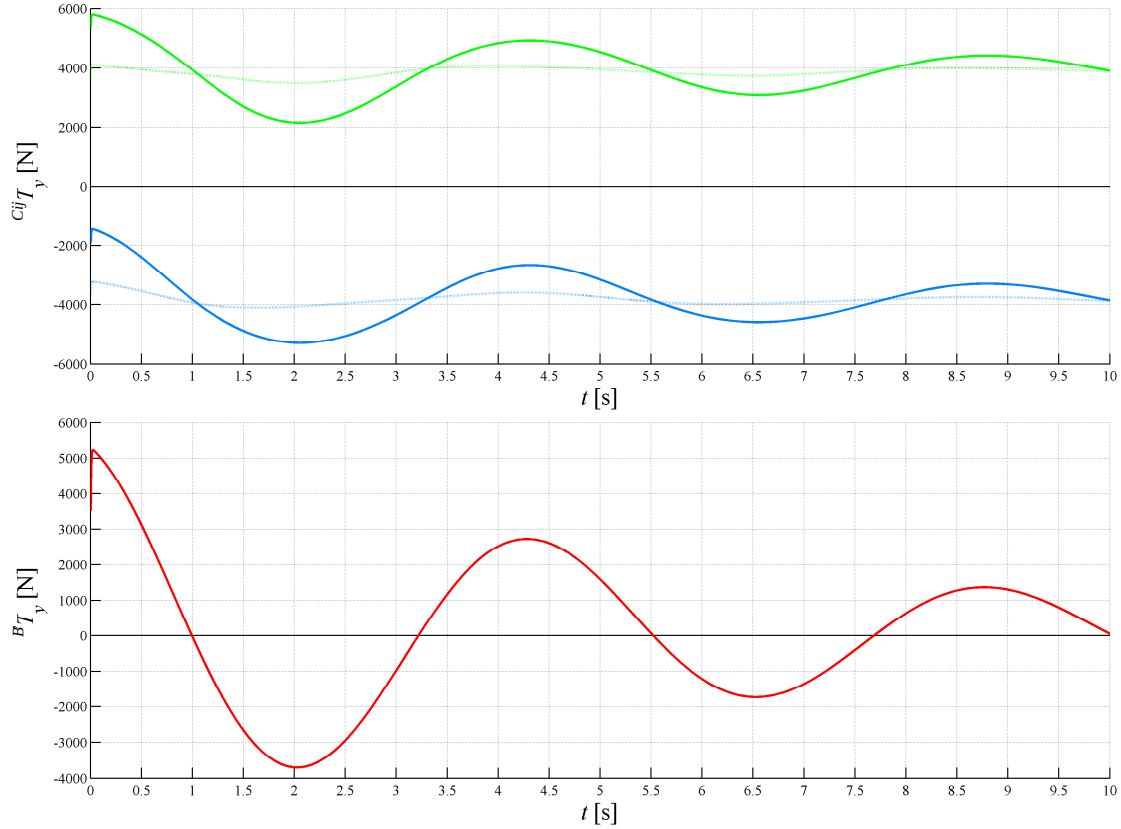

Fig. 10: Lateral creep forces.

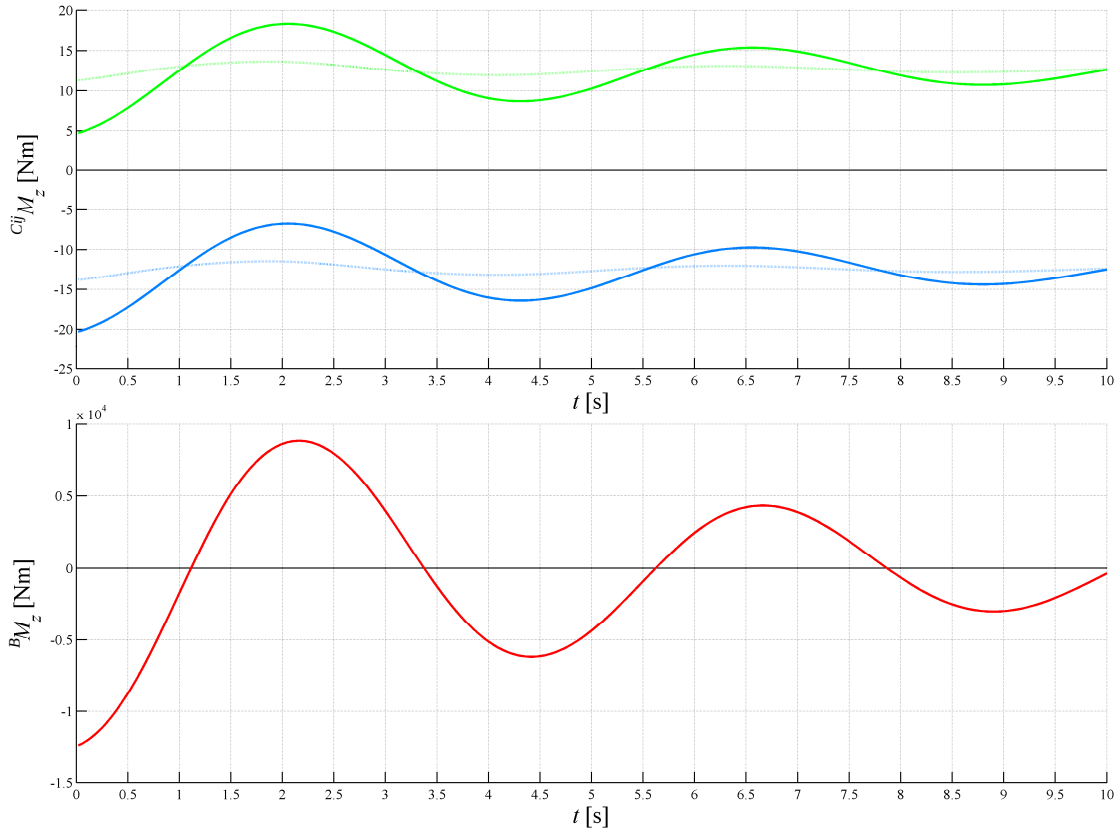

Fig. 11: Normal creep moments.

8. Results and discussion

The motion numerical solution of the loaded bogie by the half weight of the vehicle case without and with secondary suspension was made for various forward velocities on the straight railway. The lateral motion of the free biaxial bogie, i.e. without secondary suspension, moves steady approximately up to the forward velocity v = 10 [kmh^{-1}], Fig. 4. For higher velocity the bogie's motion is unsteady. The bogie with the secondary suspension is steady for every forward velocity. The lateral motion of the bogie mass center with the secondary suspension is presented as a function $y = y(t)$ and $\dot{y} = \dot{y}\left(y(t)\right)$ which is called the *phase trajectory*, Fig. 6, 7.

9. Conclusion

The mathematical model of the railway vehicle bogie was created and the numerical solution of this mathematical model was made by own developed software which allows to simulate a bogie motion in dependence on initial values. The next work will be oriented to the creation of a mathematical model of a complete railway vehicle with two doubly suspended bogies and eventually with consideration of a finite stiffness of a rail with a subsoil.

Acknowledgement

The paper was written with the support of the project MŠMT 1M0519 – Research Centre of

Rail Vehicles.

References

Byrtus M., Zeman V., Hlaváč Z. (2007) Modelling and dynamical analysis of an individual wheelset drive of a railway vehicle. *Current Problems in Rail Vehicles 2007* (Volume 1). Žilina, Slovakia, (pages 98 – 106).

Garg, V. K. & Dukkipati, R. V. (1984) *Dynamics of Railway Vehicle Systems*. Academic publisher, London, Great Britain.

Jandora R. (2007) Modelling of railway vehicle movement considering non-ideal geometry of wheels and rails. *Applied and Computational Mechanics 2007*. Hrad Nečtiny, Czech Republic (pages 489 – 498).

Johnson K. L. & Vermeulen P. J. (1964) Contact of nonspherical bodies transmitting tangential forces. *International Applied Mechanics 31* (pages 338 – 340).

Kalker, J. J. (1967) *On the Rolling Contact of Two Elastic Bodies in the Presence of Dry Friction*, Ph. D. dissertation, Delft University of Technology, Delft, Netherlands.

Moravčík, M. & Zelenka, J. (2007) Dynamic response of the vehicle running in the rail. *Current Problems in Rail Vehicles 2007* (Volume 2). Žilina, Slovakia, (pages 101 – 108).

Siegl J. & Švígler J. (2006) Vliv zpřesněného výpočtu creepových silových účinků na stabilitu pohybu dvojkolí. *Computational Mechanics 2006*. Hrad Nečtiny, Czech Republic.

Švígler, J. & Siegl, J. (2007) Contribution to modelling of contact between wheel set and curved railway. *Engineering Mechanics 2007*, Svratka, Czech Republic.